Check for updates

Geochemistry, Geophysics, Geosystems®

AGU ADVANCING EARTH AND SPACE SCIENCE

RESEARCH ARTICLE
10.1029/2021GC010288

Gas Leakage From Shallow Ponding Magma and Trapdoor Faulting at Sierra Negra Volcano (Isabela Island, Galápagos)

Alessandro Aiuppa[1], Patrick Allard[2], Benjamin Bernard[3], Francesco Maria Lo Forte[1], Roberto Moretti[2,4], and Silvana Hidalgo[3]

[1]Dipartimento di Scienze della Terra e del Mare, Università di Palermo, Palermo, Italy, [2]Université de Paris, Institut de physique du globe de Paris, CNRS UMR, Paris, France, [3]Instituto Geofisico, Escuela Politécnica Nacional, Quito, Ecuador, [4]Observatoire volcanologique et sismologique de Guadeloupe, Institut de physique du globe de Paris, Paris, France

Key Points:

- The composition and mass flux of volcanic gases from Minas de Azufre, in the Sierra Negra Caldera (Galápagos), are determined
- Fluids are interpreted as prevalently derived from a shallow (~2 km deep) magmatic sill underneath the caldera floor
- Trapdoor faults at the resurgent caldera block's margin favor magmatic gas leakage and surface discharge

Correspondence to:

A. Aiuppa,
alessandro.aiuppa@unipa.it

Citation:

Aiuppa, A., Allard, P., Bernard, B., Lo Forte, F. M., Moretti, R., & Hidalgo, S. (2022). Gas leakage from shallow ponding magma and trapdoor faulting at Sierra Negra volcano (Isabela Island, Galápagos). *Geochemistry, Geophysics, Geosystems*, *23*, e2021GC010288. https://doi.org/10.1029/2021GC010288

Received 3 DEC 2021
Accepted 7 FEB 2022

Author Contributions:

Conceptualization: Alessandro Aiuppa
Data curation: Alessandro Aiuppa
Formal analysis: Alessandro Aiuppa, Francesco Maria Lo Forte, Roberto Moretti
Funding acquisition: Alessandro Aiuppa, Silvana Hidalgo
Investigation: Alessandro Aiuppa, Patrick Allard, Benjamin Bernard, Francesco Maria Lo Forte, Silvana Hidalgo
Methodology: Alessandro Aiuppa
Project Administration: Alessandro Aiuppa, Silvana Hidalgo
Software: Roberto Moretti
Visualization: Alessandro Aiuppa, Francesco Maria Lo Forte
Writing – original draft: Alessandro Aiuppa

© 2022. The Authors.
This is an open access article under the terms of the Creative Commons Attribution License, which permits use, distribution and reproduction in any medium, provided the original work is properly cited.

Abstract We report on new volcanic gas composition results acquired in October 2017 at Minas de Azufre, a persistent fumarolic field topping the resurgent Sierra Negra caldera, in the Galápagos archipelago. Our results indicate that the Minas de Azufre fumaroles are moderately hydrous (52–64 mol.% H_2O) and rich in CO_2 (35–46 mol.%), with total sulfur (S_T) being 21–35 times less abundant than CO_2. SO_2, the most abundant S species, is released at an average rate of 19 ± 9 tons/day. Using a volatile saturation model that provides the composition of magmatic gases at equilibrium with western Galápagos basaltic melt (48 wt. % SiO_2) in the 400–0.1 MPa pressure range, we infer that Minas de Azufre fumarolic emissions consist of a mixture of (a) magma-derived gases coexisting with a melt at ~50–60 MPa and (b) shallow meteoric water. We thus propose that the fumaroles are supplied by outgassing of magma stored in a ~2 km deep sill-like reservoir underneath the caldera floor, and that the trapdoor fault system at the western margin of the resurgent caldera block acts as a preferential pathway for magmatic gas ascent and surface discharge. Our results thus suggest that, in contrast to the majority of the volcano-hosted hydrothermal systems worldwide, Minas de Azufre releases a relatively pristine magmatic gas.

Plain Language Summary Magmatic gas released by intraplate, hot-spot related volcanism can offer insight into the abundance and distribution of volatiles in the Earth's upper mantle. Unfortunately however, the available data set for hot spot magmatic gases is sparse and incomplete, due to relatively infrequent eruptions and the remote location of many hot-spot volcanoes. Here, we present novel information for the gas chemistry and emission rate at the Minas de Azufre fumarolic field, the most active persistent gas manifestation on Sierra Negra volcano, in the western part of the Galápagos hotspot. We interpret our gas observations in tandem with results of a volatile saturation model that calculates the equilibrium composition of magmatic gases coexisting with basaltic melt under P-T conditions relevant to Galápagos volcanism. From this comparison, we conclude that the Minas de Azufre fumarolic emissions are fed by degassing of basaltic magma stored in a ~2 km deep sill underneath the Sierra Negra caldera floor, and that the trapdoor fault system at the western margin of the resurgent caldera block acts as a preferential pathway for magmatic gas leakage and surface discharge. Our results are relevant to a better understanding of Sierra Negra volcano and contribute to extending the volcanic gas catalog for hot-spot volcanism.

1. Introduction

Magmatic gas delivered by intraplate, hot-spot related volcanism offers important insight into the abundance and distribution of volatiles in the Earth's upper mantle (Aiuppa et al., 2021) and hence into the rates and mechanisms of volatile exchange in and out our planet (Dasgupta & Hirschmann, 2010). Hot-spot magmatic gases have long been recognized (Gerlach, 1982; Symonds et al., 1994) to exhibit CO_2-richer (and H_2O-poorer) compositions relative to arc magmatic gases (Fischer, 2008; Fischer & Chiodini, 2015; Oppenheimer et al., 2014; Taran & Zelenski, 2015), attesting for the presence of a carbon-rich mantle reservoir (Aiuppa et al., 2021, and references therein) at depths higher than the shallow (<50 km) Depleted Mantle (DM) sampled by MORBs (Mid-Ocean Ridge Basalts; Hauri et al., 2019). Combined with the specific trace element and radiogenic isotope signatures of hot-spot volcanic rocks (Hoffman, 2003; Zindler & Hart, 1986), the composition of intraplate magmatic gases may thus provide unique information on volatiles' heterogeneities in mantle plumes. Unfortunately, however, the existing data set for hot-spot magmatic gases is still limited (Aiuppa et al., 2021), detailed information being available for only the Hawaiian (Gerlach & Graeber, 1985; Sutton & Elias, 2014), Icelandic (Pfeffer et al., 2018;

Writing – review & editing: Alessandro Aiuppa, Patrick Allard, Benjamin Bernard, Francesco Maria Lo Forte, Roberto Moretti, Silvana Hidalgo

Sigvaldsson & Elisson, 1968) and Ethiopian (Erta Ale: Sawyer et al., 2008; de Moor et al., 2013; Zelenski et al., 2013) hot spots. This paucity of data reflects the relatively infrequent eruptions and remote locations of many/most hot-spot volcanoes.

The western portion of the Galápagos archipelago, in the eastern Pacific (Figure 1), has recently been the theater of some of the most recurrent hot-spot related volcanic eruptions (Bell et al., 2021; Kurz et al., 2014; Vasconez et al., 2018). With its 10 major volcanic islands (and 21 subaerial Holocene volcanoes in total; Harpp et al., 2014), the Galápagos archipelago is thought to represent the surface expression of an upwelling mantle plume (Geist et al., 1988; see also Harpp & Geist, 2018 for a recent review) that intersects the Nazca plate ∼1,000 km off the west coast of Ecuador. Seismic imaging suggests that the plume originates from depths greater than 410 km (Hooft et al., 2003) and that its center is rooted today beneath Fernandina and Isabela islands (Villagómez et al., 2007), in the western part of the archipelago (Figure 1). These two western islands of Galápagos are thus relevant sites to investigate the chemistry and degassing of plume-sourced magmatic volatiles. Up to now, however, the chemistry of magmatic gases during an eruption on Fernandina or Isabela has not yet been measured, mostly because of the remoteness of the area and challenging access to eruption sites.

So far, the only accessible source of information on Galápagos volcanic gases has been the long-lived fumarolic field of Minas de Azufre (Colony & Nordlie, 1973). This persistent degassing area occurs within the summit caldera of the Sierra Negra shield volcano (Reynolds et al., 1995) that constitutes the southern part of Isabela island (Figure 1). Giggenbach (1996) and Goff et al. (2000) were the first to report a high SO_2/H_2S ratio in fumarolic gas emissions at Minas de Azufre, which, in combination with detectable HCl, was taken as the signature of a shallow magmatic source (Goff et al., 2000). Based on oxygen/hydrogen isotopic compositions of the fumarolic steam Goff et al. (2000) and Taran et al. (2010) inferred that the magma-supplied volatiles were extensively mixed with shallow meteoric fluids upon ascent toward the surface. However, in the late 1990s, assessing the pristine (pre-mixing) composition of the magmatic end-member and its source depth beneath the fumarolic field remained hampered by limited knowledge of the structure of the Sierra Negra plumbing system (Reynolds et al., 1995), as well as by the lack of quantitative volatile saturation models allowing to predict the pressure-related composition of H-C-O-S fluid in equilibrium with western Galapagos magma.

Here, we present novel information for the chemical composition and emission rate of volcanic gases released by the Minas de Azufre fumarolic system, which we acquired during a field work conducted in early October 2017 in the framework of the thirteenth CCVG-IAVCEI gas workshop (https://ccvg.iavceivolcano.org/workshops/workshop-2011-2017.html). We take advantage of the improved geophysical knowledge of the subsurface structure of Sierra Negra summit caldera (Amelung et al., 2000; Bell et al., 2021; Chadwick et al., 2006; Jónsson et al., 2005), as well as of new volatile saturation models that incorporate the complex sulfur behavior in magmas (Moretti et al., 2003; Moretti & Papale, 2004), to propose that degassing at Minas de Azufre is sustained by magmatic gas leakage from magma ponding at ∼2 km depth beneath the summit caldera floor.

2. Materials and Methods

2.1. Sierra Negra Volcano

Sierra Negra is a large, frequently erupting basaltic shield volcano (Reynolds et al., 1995) that occupies the southern part of Isabela island (Figure 1). Sierra Negra is, after Fernandina further to the west (Figure 1), the historically most active volcano of the Galápagos hot-spot (Reynolds et al., 1995). Its two most recent eruptions occurred in 2005 (Geist et al., 2008) and 2018 (Bell et al., 2021; Vasconez et al., 2018).

The subaerial (60 km long and 40 km wide) edifice of Sierra Negra has been modeled by protracted effusive activity over the last 7 kyr (Reynolds et al., 1995). The erupted volcanics are MgO-rich (∼4–∼7 wt %) basalts with transitional alkaline to tholeiitic affinity whose enriched Light Rare Earth Element (LREE) and incompatible trace-element compositions and radiogenic Sr and Pb signatures indicate their derivation from 5% to 15% partial melting of a garnet-bearing peridotitic plume-related source (Reynolds & Geist, 1995; White et al., 1993). This enriched "mantle plume" affinity, further corroborated by noble gas systematics (Kurz et al., 2009; Kurz & Geist, 1999), contrasts with the MORB-like signatures of magmas erupted in the central and eastern segment of the archipelago (Gibson et al., 2012; Harpp & White, 2001).

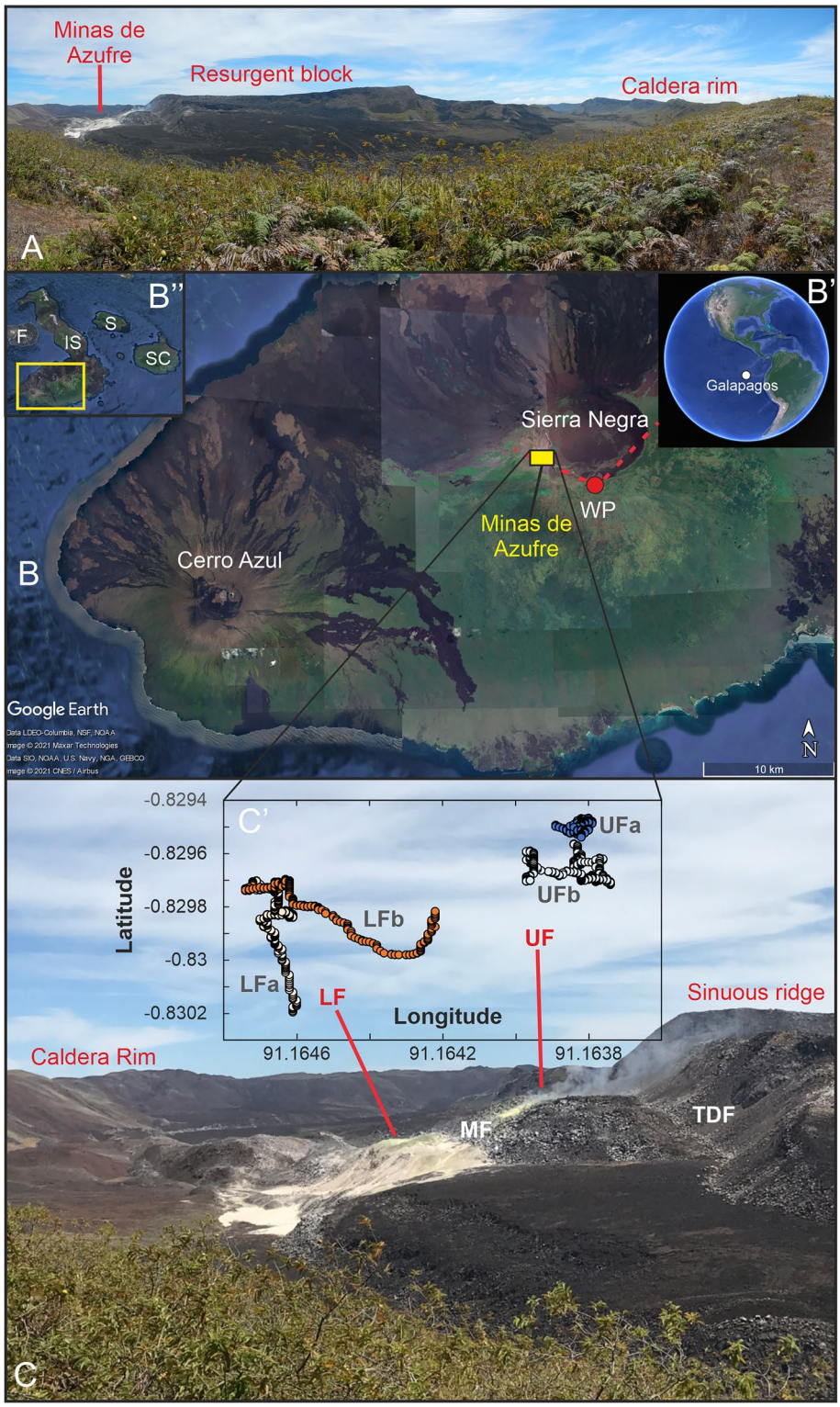

Figure 1. The study area. (a) Panoramic view of the Sierra Negra caldera (photo taken from site labeled WP in (b)), showing the Minas the Azufre fumarolic field on the western margin of the central resurgent block in the caldera; (b) Google Earth image of South Isabela island. Insets show the location of Galápagos archipelago (right) and its western/central segment (I: Isabela; F: Fernandina; S: Santiago; SC: Santa Cruz); (c) The Minas the Azufre fumarolic field. The inset shows the GPS track of our walking traverse for Multi-GAS measurements. Different symbols identify distinct parts of the fumarolic field (LF: Lower Field; MF: Middle Field; UF: Upper Field). We distinguish field sub-segments (a and b) for both the LF and UF. The fumarolic field is located on a Trapdoor Fault System (TDF) at the margin of the sinuous ridge (Goff et al., 2000; Reynolds et al., 1995).

Table 1
Gas Compositions and Fluxes

	Molar ratios						Molal fractions								
	H_2S/SO_2	CO_2/SO_2	H_2O/SO_2	CO_2/S_T	H_2O/CO_2		H_2O	CO_2	SO_2	H_2S					
LFa	0.11	34	62	31	1.8	**LFa**	0.64	0.35	0.010	0.001					
LFb	0.12	39	50	35	1.3	**LFb**	0.55	0.43	0.011	0.001					
UFa	0.31	32	36	24	1.1	**UFa**	0.52	0.46	0.014	0.004					
UFb	0.29	27	44	21	1.6	**UFb**	0.61	0.37	0.014	0.004					
	Molar Ratios						**Molal fractions**					**Fluxes (tons/day)**			
	H_2S/SO_2	CO_2/SO_2	H_2O/SO_2	CO_2/S_T	H_2O/CO_2		H_2O	CO_2	SO_2	H_2S		H_2O	CO_2	SO_2	H_2S
Mean (all data)	0.2	33	48	28	1.5	**Mean (all data)**	0.58	0.40	0.012	0.003	**Mean**	263	442	19	2
σ	*0.1*	*5*	*11*	*6*	*0.3*	***σ***	*0.05*	*0.05*	*0.002*	*0.002*	***σ***	*184*	*274*	*9*	*2*
Mean (UF)	0.3	30	40	23	1.4	**Mean (UF)**	0.56	0.42	0.014	0.004	**Mean**	219	395	19	3
σ	*0.01*	*4*	*6*	*2*	*0.4*	***σ***	*0.06*	*0.06*	*0.0004*	*0.0003*	***σ***	*134*	*233*	*9*	*2*

Note. The molar ratios in the four subsegments of the Minas de Azufre fumarolic field (LFa, LFb, UFa, UFb) are derived from the gradients of the best-fit regression lines in the gas versus SO_2 scatter plots of Figure 2. Mean molar ratios for the fumarolic field are calculated by averaging the entire data set (all data) or the Upper Field (UF) results only (as this contributes most of the emission budget). Molar fractions are calculated assuming that H_2O, CO_2, SO_2 and H_2S make up the totality of the gas phase, which is a reasonable approximation (see text). Gas fluxes are derived by scaling the average fumarolic compositions to the UV-Camera derived SO_2 flux of 19 tons/day.

The top morphology of Sierra Negra volcano is characterized by a ENE–WSW elliptical (10 × 7 km) summit caldera that has recently undergone several episodes of collapse, upheaval, and deformation (Amelung et al., 2000; Bell et al., 2021; Geist et al., 2008; Jónsson et al., 2005). The caldera hosts in its center a 14 km-long C-shaped sinuous ridge (Figure 1), interpreted as the product of a long-lived caldera floor resurgence process (Reynolds et al., 1995). Deformation and resurgence are thought to be controlled by a Trapdoor Fault (TDF) mechanism, of which the sinuous ridge would be the surface expression, with the eastern caldera floor acting as hinge zone (Amelung et al., 2000; Jónsson et al., 2005). Uplift/subsidence of the TDF block are interpreted as caused by magma pressure change inside a flat, sill-like magma reservoir emplaced at only ~2 km depth beneath the caldera floor (Bell et al., 2021; Chadwick et al., 2006).

2.2. Minas de Azufre

The Minas de Azufre fumarolic field is located on a steep scar at the western margin of the sinuous ridge (Figure 1). A series of relatively narrow benches and "moats" in the fumarolic field itself and on the adjacent caldera floor supports that the Minas de Azufre fumarolic field stands right on the main faulted boundary of the resurgent block, thereby suggesting gas ascent and fumarolic discharge are controlled by the geometry of the TDF system (Goff et al., 2000). In their 1995 survey, Goff et al. (2000) reported the presence of two fumarolic clusters (max. temperature of 208°C) marking the edges of two closely spaced N-S trending faulted blocks. Additional measurements were taken during short-lived campaigns in 2004 (Taran et al., 2010) and 2006 (Padrón et al., 2012).

3. Data

Our gas investigations were realized on 6 October 2017 under clear sky and dry weather conditions. We used a portable Multi-Component Gas Analyzer System (Multi-GAS; Aiuppa et al., 2005; Shinohara, 2005) to perform a walking traverse through the Minas de Azufre fumarolic field along the path shown in Figure 1 (bottom panel). Two fumarole clusters, thereafter referred to as Lower Field (LF) and Upper Field (UF), were actively degassing during our survey (Figure 1), with respective discharge temperatures of 139 and 273°C (Hidalgo et al., 2014). Both fields were composed of several tens of fumarolic vents and, for simplicity, we subdivide each of them into 2 subcategories (a and b) based on their location (Figure 1; Table 1). The fumarolic field in between UF and LF (Middle Field, MF; see Figure 1) was weakly fuming.

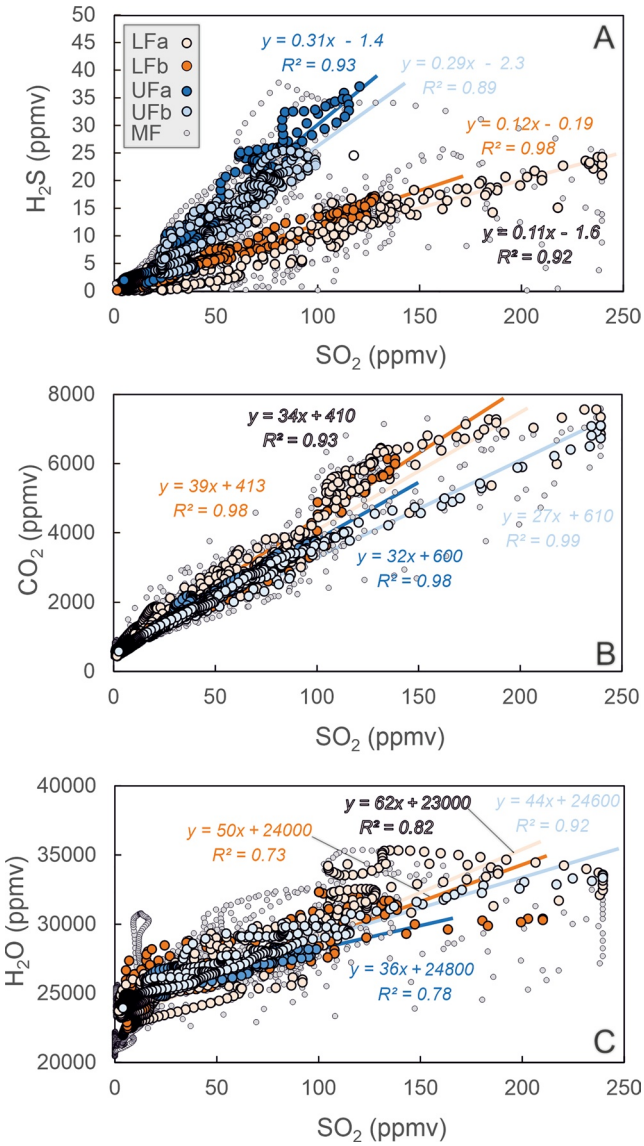

Figure 2. Multi-GAS data set. Scatterplots of co-acquired (a) H_2S versus SO_2, (b) CO_2 versus SO_2 and (c) H_2O versus SO_2 concentrations, measured with Multi-Component Gas Analyzer System during the walking traverse. Distinct segments of the fumarolic field (Figure 1c) are identified by different colors (see legend). Equations of the best-fit regression lines, calculated from data of individual sub-fields, are shown with regression coefficients.

During our walking traverse the Multi-GAS was operated in a backpack and fumarolic gas effluents were pumped in (at 1.2 l/m rate) through the hand-held inlet tubing positioned ~50 cm above the vents. Each fumarolic vent was monitored for a few minutes, so that the entire field (LF-UF) was covered in ~80 min. Our Multi-GAS device included a Gascard nondispersive infrared (NDIR) spectrometer from Edinburgh Sensors (for CO_2) and two specific electrochemical sensors (both from City Technology) for SO_2 and H_2S (see Lages et al., 2020, for a description of the most recent Multi-GAS configuration, and for details on sensor's accuracy and repeatability, calibration ranges and gas standards). The system also measured temperature (T) and relative humidity (Rh; with a KVM3/5 Galltec-Mela sensor), which were converted into H_2O concentrations using the Arden Buck equation (Tamburello, 2015). Data were acquired at 1 Hz synchronously from all sensors and stored on a Campbell CR6 datalogger. The obtained Multi-GAS data set is illustrated in Figure 2.

Synchronously to the Multi-GAS walking traverse, we operated a portable dual UV-camera system (described in Aiuppa et al., 2015), positioned at the base of the fumarolic field (Figure 3a), to determine the SO_2 emission rate from the overall fumarolic field. The UV-camera, powered by a 12-V battery and commanded via a portable PC using the Vulcamera software (Tamburello et al., 2011), acquired sets of images at 0.5 Hz for ~100 min. The instrument was equipped with two JAI CM-140GE-UV cameras sensible to UV radiation and fitted with two distinct bandpass filters centered at 310 nm (strong SO_2 absorption) and 330 nm (no SO_2 absorption) (compare panels B and B' in Figure 3). During post-processing, sets of co-acquired images (e.g., B and B') were combined (using Vulcamera) to obtain sequences of "absorbance" images (panel B' in Figure 3); these were converted into slant column amount (SCA) images using calibrations derived from calibration cells. Integration of SCA images along a cross section perpendicular to the plume transport direction yielded time series of Integrated Column Amounts (ICAs) which, multiplied by the plume speed, result in the SO_2 flux time series shown in Figure 3c. The plume speed and its temporal variations (Figure 3c; uncertainty, ±5%) were derived by tracking the motion of plume gas fronts in image sequences, using an optical flow algorithm (see Delle Donne et al., 2019). Uncertainty in the resulting SO_2 flux is assessed at ±30%

4. Results

The Multi-GAS data set, illustrated in Figure 2, provides a snapshot of the spatial heterogeneity of volcanic gas composition throughout the Minas de Azufre fumarolic field. The scatterplots compare sets of co-acquired (a) H_2S versus SO_2, (b) CO_2 versus SO_2 and (c) H_2O versus SO_2 concentration couples. Colors of the symbols identify measurements taken in distinct portions of the fumarolic field and thus respectively refer to subfields LFa, LFb, UFa and UFb (see Figure 1). For each of these subfields, strong correlations between SO_2 and other gas species are observed (Figure 2), implying relatively constant gas/SO_2 ratios. These ratios (listed in Table 1 and all given on a molar basis) are derived from the gradients of the best-fit regression lines shown in Figure 2 (with equations and regression coefficients). Gray dots identify measurements taken in the walking path between LF and UF (in the MF area; Figure 1), in which correlations between the different gas specifies are somewhat weaker. As degassing in the MF area was very sluggish, these measurements more likely represent distal and variable mixing of the plumes issuing from the UF and LF fumarolic fields, which were occasionally dispersed tens of meters away from the vent(s) by erratic change in wind direction and mixed in the background atmosphere. The gray dots consistently overlap the compositions of UF and LF fields.

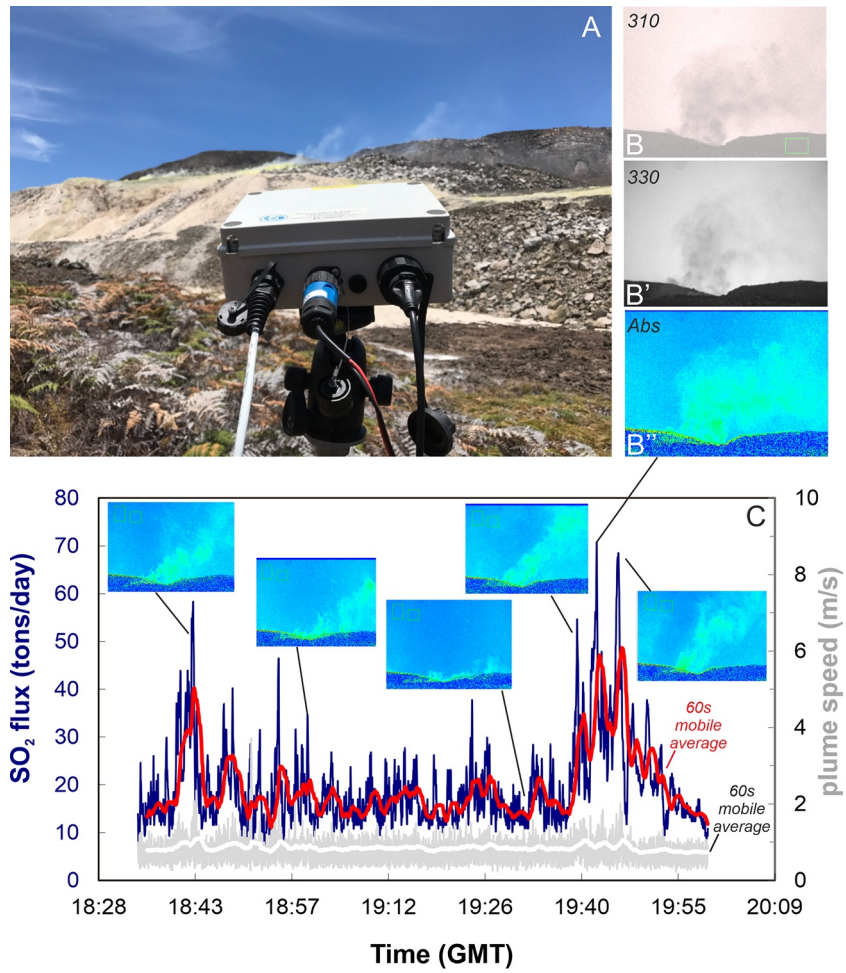

Figure 3. UV-camera data set. (a) The UV camera system targeting Minas de Azufre fumarolic emissions in the background; (b) panels B and B' are examples of co-acquired images with filters centered at 310 nm (strong SO_2 absorption) and 330 nm (no SO_2 absorption), respectively. Combination of the two yields the "absorbance" image of panel B"; (c) time series of SO_2 flux (blue, with 60s mobile average in red) and plume speed (gray, 60s mobile average in white). Insets show absorbance images taken at specific time intervals.

Our results confirm previous indications (Giggenbach, 1996; Goff et al., 2000; Padrón et al., 2012; Taran et al., 2010) that SO_2 is the prevalent sulfur gas species in Minas de Azufre fumaroles (Table 1). However, compared to these earlier studies based on direct fumarole sampling at only a few vents, the rapidity of Multi-GAS sensing allowed us to analyze several tens of degassing vents in sequence and hence to capture with great detail the spatial heterogeneity of H_2S/SO_2 ratios in the field. We find significant compositional differences between the LF and UF fumarolic fields: compared to UF, the LF exhibits lower H_2S/SO_2 ratios (0.11–0.12 vs. 0.29–0.31; Figure 2a), higher CO_2/SO_2 (34–39 vs. 31–35; Figure 2b) and CO_2/S_T ($S_T = SO_2 + H_2S$) ratios (27–32 vs. 21–24; Table 1). LF also displays slightly higher H_2O/SO_2 ratios (50–62) than UF (36–44; Figure 2c), while H_2O/CO_2 ratios are similar at both fields (1.3–1.8 and 1.1–1.6, respectively; Table 1).

Gas molar fractions (Table 1) were calculated by assuming that H_2O, CO_2, SO_2 and H_2S make up the totality of the gas phase (other species, such as N_2 and HCl, were found to occur at minor levels in Minas de Azufre fumaroles; Goff et al., 2000; Taran et al., 2010). Our results demonstrate a volcanic gas phase containing 52–64 mol% of H_2O, 35%–56% of CO_2, and much lower amounts of SO_2 (1.0%–1.4%) and H_2S (0.1%–0.4%).

Figure 3 shows a temporal record of the SO_2 flux, as derived from our ~100 min-long UV-camera recording. The absorbance images displayed in the figure clearly identify the volcanic plume (indicated by green-yellow tones on blue background) gently lofting above the sinuous ridge's upper rim, and then dispersing to the right of the

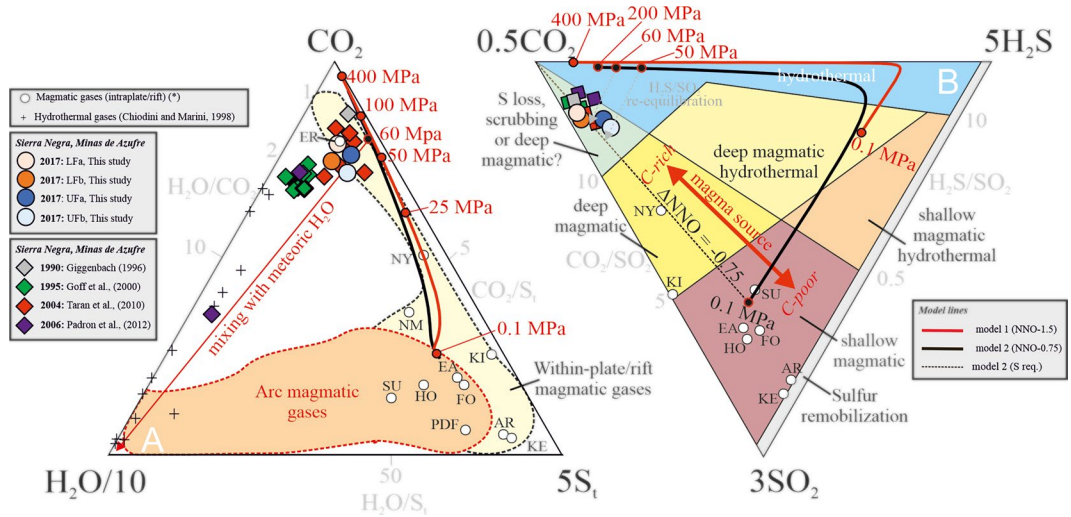

Figure 4. Triangular classification plots of volcanic gas. (a) H_2O/10-CO_2-5S_T triangular plot, comparing our chemical results for Minas de Azufre fumarolic gas in 2017 with previously obtained data (1990–2006). The compositional domains of within-plate/rift and arc magmatic gases are from Aiuppa (2015), while crosses are a selection of hydrothermal gases (Chiodini & Marini, 1998). Representative compositions of magmatic gases from intraplate/continental rift contexts are from Aiuppa (2015) except where indicated. ER: Erebus, NY: Nyiragongo; NM: Nyamuragira; KI: Kilauea; EA: Erta Ale; FO: Pico do Fogo (Cape Verde; Hernández et al., 2015); SU: Surtsey; HO: Holuhraun (Pfeffer et al., 2018); PDF: Piton de la Fournaise; AR: Ardoukoba; KE: Kilauea East Rift Zone. The red and black solid lines represent the modeled gas compositions in our Model runs 1 and 2 for closed-system magma decompression at 1,300°K in the 400–0.1 MPa pressure range (input parameters listed in Table 2), under redox conditions of either ΔNNO = −1.5 (model 1) and ΔNNO = −0.75 (model 2). Small circles (red/black) on the model lines identify model gas compositions at specific pressures (indicated in MPa). The red arrow indicates mixing between uprising magmatic gas separated from the magma at 60 MPa and a pure meteoric water component; (b) 0.5CO_2-3SO_2-5H_2S triangular plot. The colored areas refer to the gas classification fields of Stix and de Moor (2018) except for the light green area labeled as "S loss, scrubbing or deep magmatic"?, that can refer to the compositional field of either (i) S-depleted, "scrubbed hydrothermal gases, or (ii) CO_2-rich, S-poor deeply equilibrated magmatic gas (see text). Model lines 1 and 2 are as in (a). The dashed gray lines, referred as "H_2S/SO_2 re-equilibration," describe the evolution of the uprising magmatic gas while its SO_2/H_2S ratio re-equilibrates (at constant CO_2/S_T and redox at ΔNNO = −0.75) during decompression from 50 to 60 MPa (magmatic sill) down to 0.1 MPa. Intraplate-continental rift magmatic gases (white circles) range from C-rich to C-poor, depending on the C-enriched or C-depleted signature of their mantle source (Aiuppa et al., 2021).

camera's field of view (e.g., southward). The plume speed (Figure 3c) was relatively constant at 0.9 ± 0.3 m/s. The computed SO_2 flux varies from 6.2 to 71 tons/day, with a mean at 19 ± 9 tons/day. Qualitative inspection of the images suggests that the SO_2 flux was mainly supplied by degassing from the UF.

The fluxes of other volatiles (H_2O, CO_2, and H_2S) are quantified by combining the time-averaged SO_2 flux with the mean composition of the Minas de Azufre fumaroles (Table 1). We provide two separate estimates in Table 1 when using the average gas composition from either the entire field (LF + UF) or the UF only (the largest SO_2 flux source, see above). Under these two conditions we assess the H_2O, CO_2, and H_2S fluxes at 219–263, 395–442 and 2–3 tons/day, respectively (Table 1).

5. Discussion

Owing to its remoteness, the Minas de Azufre fumarolic field has only rarely been targeted by volcanic gas investigations in the last decades. Our 2017 results indicate a fumarolic gas composition broadly consistent with previous reports in 1990 (Giggenbach, 1996), 1995 (Goff et al., 2000), 2004 (Taran et al., 2010) and 2006 (Padrón et al., 2012; Figure 4). More specifically, in a H_2O-CO_2-S_T triangular diagram (Figure 4a) our data plot on the CO_2-rich side of the compositional domain of within-plate/rift magmatic gases (Aiuppa, 2015) and overlap with the composition of the 2004 samples reported by Taran et al. (2010). In contrast, our results indicate a less hydrous gas phase than reported by Goff et al. (2000) and Padrón et al. (2012) (Figure 4a).

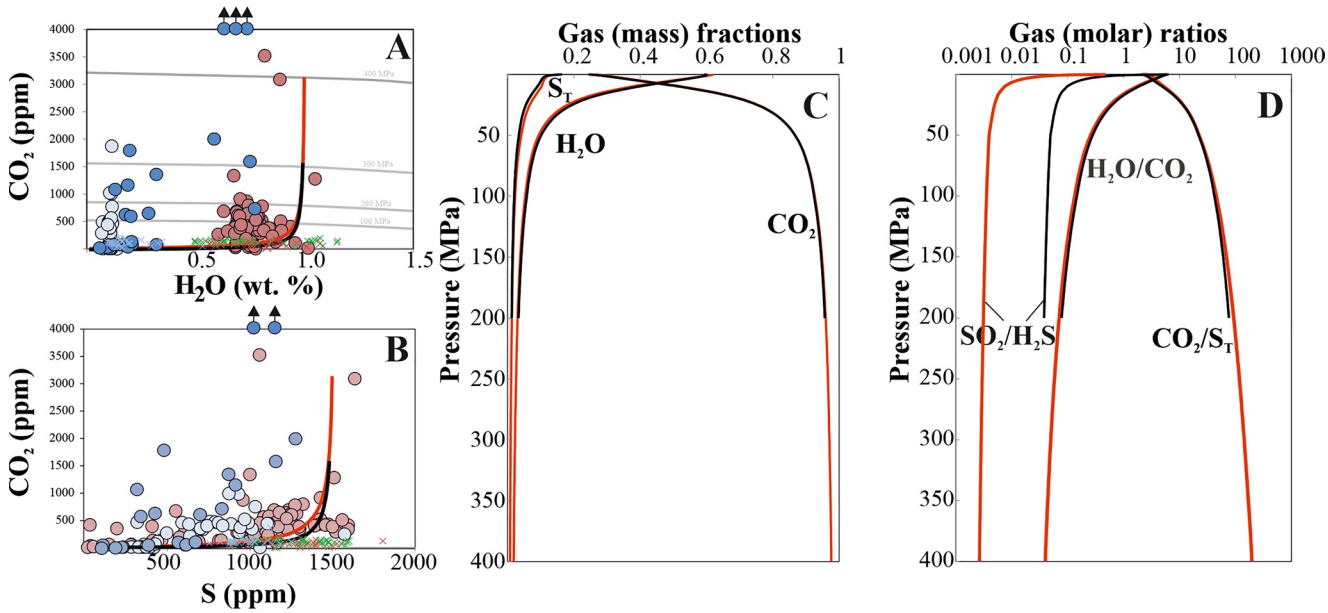

Figure 5. Result of degassing model calculations. Modeled dissolved CO_2 and H_2O contents in the melt, compared with the measured dissolved contents in olivine-hosted melt inclusions from Fernandina (red circles) Santiago (blue circles) and Floreana islands (data from Koleszar et al., 2009 and Gleeson et al., 2022). The composition of Galápagos submarine glasses (all data from Peterson et al., 2017) are also shown by crosses (red, Fernandina group; green, Sierra Negra group; blue, eastern islands-Depleted Mantle group). All model calculations were made using the volatile saturation model of Moretti et al. (2003). Solid red line: Model 1; Solid black line: Model 2. Model run starting conditions are summarized in Table 2. (b) Same as (a) but comparing CO_2 versus S contents in model runs with melt inclusion data. (c) Model-predicted pressure dependence of magmatic gas concentrations (given in mass fractions) at equilibrium with the melt in the 400 to 0.1 MPa pressure range; (d) Same as (c) but for the molar gas ratios of the magmatic gas phase. Model 2 produces higher equilibrium SO_2/H_2S ratios, reflecting the more oxidising conditions considered in this run.

In the CO_2-SO_2-H_2S classification diagram of Stix and de Moor (2018) our gas results in 2017 cluster, together with the 1990-1995-2004-2006 samples, in a relatively narrow area of CO_2-rich and H_2S-poor compositions (Figure 4b). This area, originally classified as "S loss, scrubbing" by Stix and de Moor (2018), would correspond to that of volcanic gas that experienced substantial subsurface loss of reactive sulfur species during hydrothermal reactions (e.g., reactions with meteoric/hydrothermal fluids and subsurface rocks) and consequently reached the surface with enhanced CO_2/S_T ratio. However, considering the high SO_2/H_2S ratio of Minas de Azufre fumaroles (Table 1), it is equally possible that the measured high CO_2/S_T ratios instead reflect a direct gas supply from magma stored at a depth where poorly soluble CO_2 is preferentially exsolved and degassed relatively to S (e.g., Aiuppa et al., 2007). This latter hypothesis of a deep magmatic signature, rather than the bearing of hydrothermal interactions, was privileged by Goff et al. (2000) but remained untested owing to the lack (at that time) of a quantitative C-O-H-S degassing model relevant to Sierra Negra magmas. In the following we attempt at resolving the magmatic versus hydrothermal nature of the Minas de Azufre fumarolic gas using a volatile saturation model.

5.1. Volatile Degassing Modeling Applied to Western Galápagos Magmas

We use the volatile saturation model of Moretti et al. (2003; see also Code Availability) to calculate the C-O-H-S equilibrium composition of magmatic fluids at T-P-X conditions relevant to magmas supplying the activity of Sierra Negra volcano (Figure 5). This model has been applied to other volcanoes with widely different magma compositions (Aiuppa et al., 2007, 2010, 2017; de Moor et al., 2016; Edmonds et al., 2010; Marini et al., 2011; Moretti, Arienzo, Civetta, Orsi, & Papale, 2013; Moretti, Arienzo, Civetta, Orsi, & Antonio, 2013; Moretti et al., 2018; Oppenheimer et al., 2011; Pino et al., 2011), and more details on its quantitative background can be found in Moretti et al. (2003), Moretti and Papale (2004) and Papale et al. (2006).

Using a volatile saturation model requires independent knowledge of input variables such as the melt composition (major elements, volatiles, redox conditions), temperature and initial pressure. This information is typically derived from pre-eruptive magma storage conditions recorded in primitive melt inclusions (e.g., Aiuppa et al., 2007, 2010; Spilliaert et al., 2006). Unfortunately, melt inclusion information is not available neither for

Table 2
Data Input Parameters of Our Degassing Model Runs

	Initial P (MPa)	T (°K)	Redox (ΔNNO)	Log fO_2	SiO_2 (wt%)	TiO_2 (wt%)	Al_2O_3 (wt%)	$(FeO)_T$ (wt%)	MnO (wt%)	MgO (wt%)	CaO (wt%)	Na_2O (wt%)	K_2O (wt%)	H_2O (wt%)	CO_2 (wt%)	S (wt%)
Model 1	400	1300	−1.5	−11.4	48	2.7	15.4	10	0.1	8.2	11.7	2.3	0.3	1	0.4	0.15
Model 2	200	‘‘’’	−0.75	−10.6	‘‘’’	‘‘’’	‘‘’’	‘‘’’	‘‘’’	‘‘’’	‘‘’’	‘‘’’	‘‘’’	‘‘’’	‘‘’’	‘‘’’

Note. Parental melt composition (major and volatile elements) is represented by the most primitive olivine-hosted melt inclusions on Fernandina island (Koleszar et al., 2009). All runs simulate magma decompression under isothermal conditions (1,300 °K) from an initial pressure of either 400 (Model 1) or 200 (Model 2) MPa down to atmospheric conditions (0.1 MPa). Redox conditions are kept at 1.5 (Model 1) to 0.75 (Model 2) log units below the Nickel Nickel Oxide (NNO) buffer (ΔNNO of −1.5 and −0.75, respectively). See text for discussion.

Sierra Negra volcano nor for any other volcano on Isabela island. We therefore initialise our model calculations using major element compositions and volatile contents measured in olivine-hosted melt inclusions from the nearby Fernandina volcanic island (Figures 5a and 5b; data from Koleszar et al., 2009). The validity of this indirect approach is justified by the following arguments: (a) the close proximity of Fernandina and Isabela islands, right above the centre of the Galápagos plume hot spot (Hooft et al., 2003; Villagómez et al., 2007); (b) the plume-related noble gas signature measured for both islands, in contrast to the MORB-like signature for the eastern islands (Kurz & Geist, 1999; Kurz et al., 2009; Taran et al., 2010); (c) the trace-element and radiogenic (Sr-Nd-Pb) isotope compositions of erupted volcanics from both islands which indicate a common plume-related mantle source component, enriched in incompatible trace elements (ITE) and radiogenic Sr (Gibson et al., 2012; Harpp & White, 2001; White et al., 1993), and (d) the similarity of H_2O and S contents measured in submarine basaltic glasses dragged in the proximity of the two islands (Peterson et al., 2017; Figures 5a and 5b). Instead, a less enriched mantle source has been shown to prevail under the eastern part of the archipelago (Harpp & White, 2001; Peterson et al., 2017), as represented by the H_2O-ITE-poor melt inclusions from Santiago island (Koleszar et al., 2009) and from the Depleted Group of basaltic glasses (Peterson et al., 2017; Figures 5a and 5b). The Floreana island melt inclusions (Gleeson et al., 2022) plot in an intermediate compositional field between Fernandina and Santiago (Figure 5a).

The model input conditions are summarised in Table 2. Model runs (1–2) were performed using as parental melt composition (major and volatile elements) the average composition of the two most primitive and undegassed melt inclusions from Fernandina island analysed by Koleszar et al. (2009). This parental melt has H_2O (1.0 wt%) and S (0.15 wt%) contents (Figures 5a and 5b) that match the upper H_2O and S concentrations measured in Sierra Negra submarine basaltic glasses (0.498–1.15 wt% and 0.089–0.159 wt%, respectively; Peterson et al., 2017), but is definitely richer in CO_2 (0.4 wt%) than the submarine basalts, erupted under a lower confining pressure. Runs were performed by simulating magma decompression from an initial pressure of either 400 MPa (Model 1) or 200 MPa (Model 2) down to atmospheric conditions (0.1 MPa), under isothermal (temperature kept constant at 1,300°K) and closed-system conditions (i.e., gas and melt continuously re-equilibrating during the decompression path). Equilibrium compositions of the melt and the coexisting gas phase were calculated at each step throughout the decompression path. In Model 1 redox conditions are fixed at 1.5 log units below the Nickel Nickel Oxide (NNO) buffer (ΔNNO = −1.5), in order to match the oxygen fugacity ($\sim 10^{-11.4}$ bar) for Fernandina magmas inferred by Koleszar et al. (2009) when modelling the sulphur solubility at sulfide saturation. In Model 2, we assume more oxidised (ΔNNO = −0.75) redox conditions in order to account for recent finding that mantle plumes are generally oxidised (Moussallam et al., 2019). These more oxidised conditions are also more consistent with the high SO_2/H_2S signature of Minas de Azufre fumaroles (see below) and with Fe oxidation state measurements that point to redox conditions ranging between ΔNNO = −0.6 and ΔNNO = 0 in glass samples from the Galapagos Archipelago (Peterson et al., 2015).

Results of our model calculations are illustrated in Figure 5. Figures 5a and 5b show that the modelled melt-volatile compositions reproduce quite well the range of volatile contents measured in Fernandina's melt inclusions analysed by Koleszar et al. (2009), especially for CO_2 and S (Figure 5b). In Figure 5a the trends from both Models 1 and 2 plot towards the high H_2O range of the melt inclusion population, suggesting that many of the melt inclusions may have trapped dehydrated melt flushed by deeper sourced CO_2-rich bubbles (Caricchi et al., 2018). The modelled equilibrium gas compositions (Figures 5c and 5d) are similar in both model runs (1 and 2) and highlight a CO_2-rich gas phase prevailing at high to moderate pressure and evolving to H_2O-richer (>50 wt%)

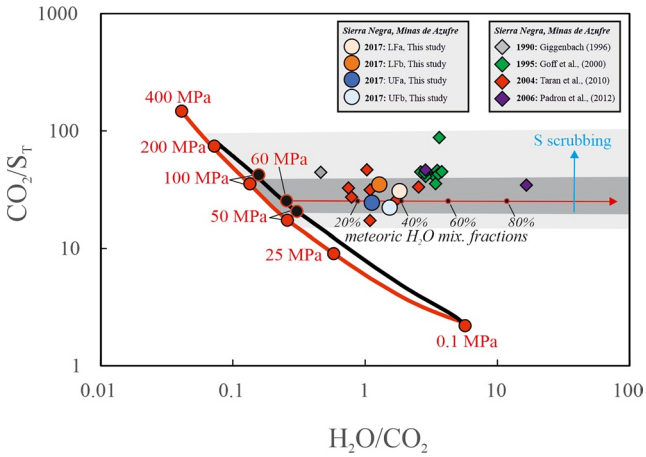

Figure 6. Observed versus modeled gas compositions. H_2O/CO_2 versus CO_2/S_T scatter plot comparing the Minas de Azufre gas data with model-derived degassing trends (see Figure 4 for legend and symbols). The Minas de Azufre fumarolic gases (this study and previous work) display relatively steady CO_2/S_T ratios, irrespective of more variable H_2O/CO_2 ratios. They are interpreted as mixtures of (i) magmatic gas released from the sill-like reservoir underlying the Sierra Negra caldera floor at ca. 2 km depth (50–60 MPa equilibrium pressure) and (ii) pure steam from heated meteoric water. The mixing line is shown by the red arrow, with meteoric H_2O mixing fractions indicated. The influence of hydrothermal scrubbing of magmatic sulfur (light blue vertical arrow) is inferred as negligible in 2017 (this study) and 2004 (Taran et al., 2010), whilst it may have contributed to the higher CO_2/S_T ratios measured in H_2O-enriched gas samples in 1995 (Goff et al., 2000) and 2006 (Pádron et al., 2012).

compositions at lower (<20 MPa) pressures. The more oxidised conditions in Model 2 result in slightly more hydrous gases and systematically higher SO_2/H_2S ratios compared to Model 1 (Figure 5d). Modelled CO_2/S_T and H_2O/CO_2 ratios are negatively correlated (Figures 5d and 6) and evolve quite similarly in the two model runs (Model 2 resulting in slightly higher H_2O/CO_2 ratio).

5.2. Origin of the Minas de Azufre Gas

Comparing our results with the modeled equilibrium gas compositions during magma decompression, as attempted in Figures 4 and 6, offers quantitative clues on the origin of the Minas de Azufre fumarolic gases. We find that the measured gas compositions (this study and previous ones) plot to the right (toward more H_2O-rich compositions) of the modeled degassing trends. This observation agrees with H-O isotopic evidence that most of the fumarolic steam is non-magmatic and rather derives from meteoric water vaporised in the subsurface (Goff et al., 2000; Taran et al., 2010).

Instead, two lines of evidence support a magmatic origin of both CO_2 and S. First, the high prevalence of SO_2 over H_2S in the fumaroles (Figure 4b) points to little sulfur scrubbing during hydrothermal reactions in the subsurface since SO_2 is much more soluble than H_2S in liquid water and would thus be preferentially removed through such reactions (e.g., Stix & de Moor, 2018). Instead, the measured mean H_2S/SO_2 ratio of 0.2–0.3 (Table 1), corresponding to SO_2/H_2S of 3–5, is identical to the ratio of the modeled equilibrium magmatic gas phase at near surface conditions (~0.2 at 0.1 MPa pressure; Figure 4b) for $\Delta NNO = -0.75$ (Model 2). Second, the measured CO_2/S_T ratios of Minas de Azufre fumaroles are relatively constant irrespective of H_2O/CO_2 variations (Figure 6). This strongly suggests no or limited S scrubbing while the rising magmatic gas interacts with infiltrating meteoric water; otherwise, CO_2/S_T would decrease as H_2O/CO_2 increases.

Hence, we propose that the CO_2/S_T ratios of the fumarolic gas are scarcely (if any) affected by hydrothermal S processing, and may rather reflect the conditions of gas separation from the magma body underlying the caldera floor. According to the modeled pressure dependence of CO_2/S_T ratio in the gas phase at equilibrium with decompressing magma (Figure 5d), the mean CO_2/S_T ratio of 28 for the whole fumarolic field (Table 1) constrains pressures of 79 ± 14 (Model 1) and 63 ± 10 MPa (Model 2) for the ultimate gas-melt equilibrium prior to gas separation from the magma body. At that point we favor Model 2 as being more representative of the magma conditions at Sierra Negra since its more oxidized redox conditions well reproduce the SO_2-rich signature of the Minas de Azufre fumarolic gas, whereas Model 1 ($\Delta NNO = -1.5$) does not (Figure 5b). In this framework, the CO_2/S_T ratio of 23 for the UF (Table 1), the portion of the fumarolic field that contributes the main fraction of the gas output (Figure 3), would yield a slightly lower degassing pressure of 51 ± 2 MPa. In summary, we propose that the Minas de Azufre fumarolic gas is best interpreted as being supplied by the outgassing of magma stored at about 50–60 MPa pressure. Such a magma/gas separation pressure corresponds to a source depth of ~1.9–2.2 km. We emphasize that this independent estimate nicely fits with the ~2 km depth of the sill-like magma reservoir underlying the caldera floor as inferred from both geodetic and petrological data (Bell et al., 2021 and references therein).

Our model calculations (Model 2) show that, at 60 MPa pressure, the equilibrium magmatic gas phase would consist of ~78% CO_2, ~18% H_2O and ~4% S_T. Comparing with the "mean" composition of Minas de Azufre fumaroles (40% CO_2, 58% H_2O and 1.2% S_T; Table 1), simple mass balance calculation implies that the fumarolic fluid in 2017 can well be explained by the shallow mixing of magmatic gas upraising from 60 MPa with meteoric water in respective mass proportions of 75%–60% and 25%–40% (Figure 6). The more hydrous compositions measured in 1995 (Goff et al., 2000) and 2006 (Padrón et al., 2012) imply greater mixing proportions of meteoric water (from ~50% to >80%; Figure 6). An even higher extent of meteoric dilution was inferred from the stable isotope ratios of fumarolic steam in 2006 (Taran et al., 2010).

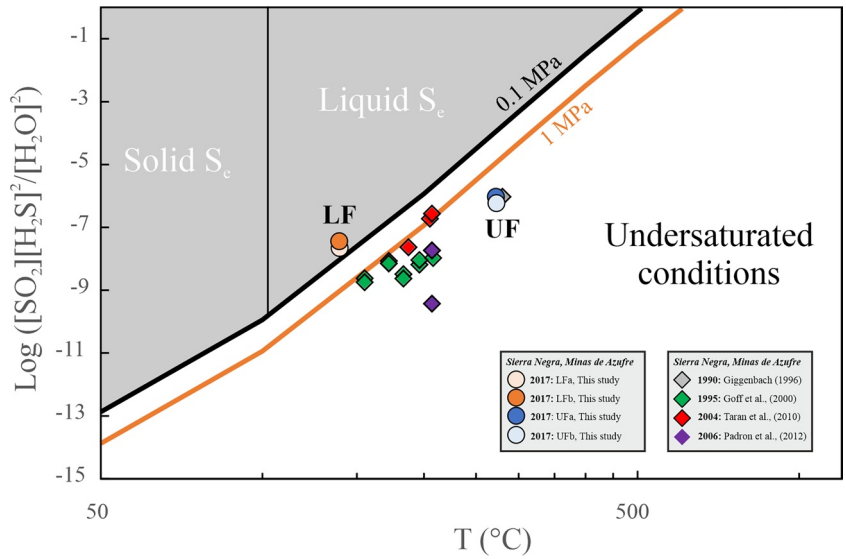

Figure 7. Modeling elemental sulfur deposition. Saturation state of Minas de Azufre fumaroles with respect to the deposition of elemental sulfur (saturation curves at 1 bar and 10 bar drawn from equilibrium constant of reaction 1 as in Giggenbach (1987).

5.3. UF Versus LF Chemical Diversity

The UF and LF fumarolic fields slightly differ in their H_2S/SO_2 and CO_2/S_T ratios (Table 1; Figures 2, 4, and 6). Because their H_2O/CO_2 ratios are indistinguishable (Table 1), these compositional differences cannot be explained in terms of distinct magmatic versus meteoric mixing proportions (see Figure 6). Instead, the two fumarolic fields differ in their spatial position and maximum emission temperature, 139°C at LF and 273°C at UF as measured in 2017. As its name actually means, the Minas de Azufre fumarolic field is characterized by abundant deposits of elemental sulfur that have been economically exploited (Colony & Nordlie, 1973). The lower H_2S/SO_2 ratios and somewhat higher CO_2/S_T ratios at LF may thus reflect partial sulfur precipitation favored by the lower exit gas temperature in this field. Elemental sulfur deposition/remobilization occurs via the reaction (Giggenbach, 1987):

$$SO_2 + 2H_2S \leftrightarrow 3S_e + 2H_2O \quad (1)$$

which consumes twice more H_2S than SO_2 and can thus modify significantly the H_2S/SO_2 ratio of the residual gas. In Figure 7 we tested the saturation state of Minas de Azufre fumaroles with respect to the deposition of elemental sulfur, using thermodynamic data from Giggenbach (1987) for the equilibrium constant of reaction (1). We find that while the hotter UF fumaroles plot in the undersaturated field, the LF fumaroles do plot to the left of the saturation line at 0.1 MPa, implying that elemental sulfur is actively deposited at the discharge conditions, in agreement with field observations. Therefore, we propose that near-surface elemental sulfur deposition controls the (minor) LF versus UF compositional differences in terms of H_2S/SO_2 and CO_2/S_T ratios (Table 1). Enhanced sulfur precipitation from LF fumarolic gases, together with their lower discharge temperatures, can be explained by their more peripheral location relative to the main gas upstream (forced by the morphology of the TDF system; Figure 8, see below), favoring more effective gas cooling and air dilution.

5.4. Magma Budget

If, as our data suggest, the bulk SO_2 emissions from Minas de Azufre are magma-derived and are not or little affected by hydrothermal scrubbing (except for some minor elemental sulfur deposition at LF, see above), then the UV-camera based SO_2 flux can be used to quantify the rate of magma supply to and degassing from the shallow (~2 km deep) Sierra Negra magma reservoir. In our calculations, we consider a magma density of 2750 kg/m^3 and a 5% crystal content (Reynolds & Geist, 1995). We assume that the magma supplying the sill contains 0.15 wt.% S (Table 2). At the reservoir conditions (50–60 MPa), our model calculations imply ~0.14 wt. % S is still dissolved in the melt (Figure 5b). Hence, ~100 mg of S can be outgassed per kg of magma supplied to

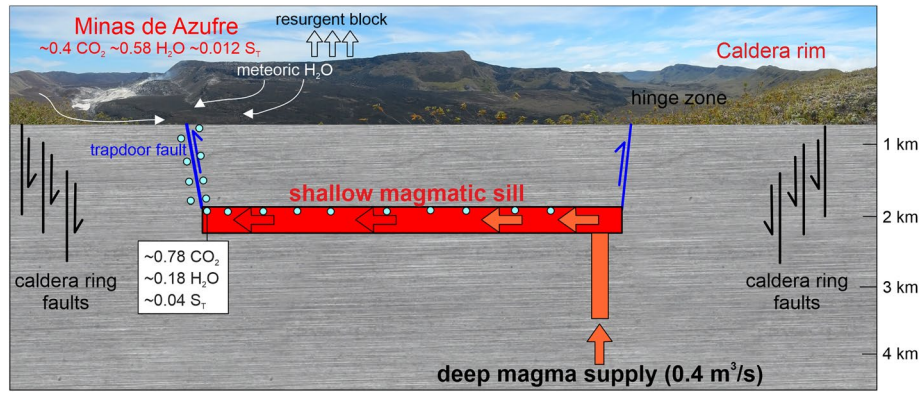

Figure 8. Conceptual model. Schematic cross-section through the Sierra Negra caldera, showing the sill-like magma storage zone at about 2 km depth (adapted from Bell et al., 2021) and our interpretative framework of magmatic gas leakage through the western trapdoor fault (TDF), variably diluted by meteoric water, that controls the chemical composition and mass output of volcanic gas at Minas de Azufre fumarolic field. The rate of magma replenishment of the sill-like reservoir is inferred from the mean SO_2 output we measured in 2017 and the mass fraction of exsolved sulfur available in this reservoir (at 50–60 MPa pressure). See the text for discussion.

the sill-like reservoir. From these numbers, we infer that a magma supply (degassing) rate of $3.6{\cdot}10^4$ m^3/day (or 0.4 m^3/s) is required to account for the SO_2 output of 19 tons/day from Minas de Azufre (Table 1).

One can safely consider the SO_2 flux of 19 tons/day measured in 2017 as representative for the long-term degassing regime at Minas de Azufre. As a matter of fact, such a flux is intermediate between the time-averaged value of ∼40 tons/day inferred from satellite-based (OMI) survey (Fischer et al., 2019) – although this was biased by the brief but intense emissions during the 2005 eruption – and the few SO_2 flux values previously measured on site (11 tons/day in June 2006, Padrón et al., 2012; 5–15 tons/day in May 2014, Hidalgo et al., 2014). Now, if we extrapolate the magma supply rate of $3.6{\cdot}10^4$ m^3/day (computed from a SO_2 flux of 19 tons/day) over the 13 years long unrest period separating the 2005 eruption and the June-August 2018 eruption (Bell et al., 2021), we obtain a total supplied magma volume of ∼0.17 km^3. This is in striking agreement with the lava volume erupted in 2018 (0.141 ± 0.071 km^3; Vasconez et al., 2018), but also with the estimated volume of magma accumulated in the sill according to geophysical modeling of the 2005–2018 pre-eruptive inflation phase (∼0.21 km^3; Bell et al., 2021).

6. Conceptual Model and Conclusions

Our observations and models are synthetized in the interpretative conceptual model of Figure 8. We propose that the Minas de Azufre fumarolic field at Sierra Negra volcano is supplied by magmatic gas leakage from the ∼2 km deep magmatic sill identified beneath the caldera floor (Bell et al., 2021). According to our calculations, deeper derived magma is supplied at an average rate of ∼0.4 m^3/s to the sill during volcano quiescence. This deep magma supply leads to gas bubble accumulation in the shallow sill during inter-eruptive periods, as indicated by gravity changes (Vigouroux et al., 2008). Seismic and geodetic evidence (Bell et al., 2021) show that both magma and gas progressively accumulate in the sill, leading to gradual pressure build-up, caldera inflation, and ultimately dyke emplacement shortly prior and during eruption. However, as our novel data highlight, magmatic gas leakage from the sill persists during volcano quiescence, sustaining the fumarolic gas discharge at Minas de Azufre. This implies that the TDF system, located on the western side of the sinuous ridge at the margin of the resurgent block (Figure 8), remains open enough to act as a preferential pathway for the magmatic gas leakage feeding the fumarolic field. We estimate that, along with ∼19 tons of SO_2, ∼395–442 tons of magmatic CO_2 and ∼65 tons of magmatic H_2O (calculated from the H_2O/S mass ratio of ∼3.5 in the magmatic gas phase at 50–60 MPa) are daily transferred from the sill to the fumarolic system. Since the measured H_2O flux from Minas de Azufre reaches ∼220–265 tons/day, we infer that ∼150–200 tons/day of vapourized meteoric water get admixed to the rising magmatic gas, which easily accounts for the prevalent meteoric isotopic composition of the emitted steam (Goff et al., 2000).

One corollary of our interpretation that the Minas de Azufre fumaroles are sourced by degassing of the shallow magmatic sill emplaced beneath Sierra Negra caldera is that the H_2S/SO_2 ratio of the magmatic gas fully

re-equilibrates along its ascent from the 50–60 MPa initial pressure to atmospheric discharge at 0.1 MPa (Figure 4b). As a matter of fact, the emitted gases have H_2S/SO_2 ratios that closely match those calculated at 0.1 MPa (model 2), whereas the modeled gas phase equilibrated at 50–60 MPa is richer in H_2S (see the "H_2S/SO_2 re-equilibration lines" in Figure 4b). In the near surface, and especially at the colder LF vents, the H_2S/SO_2 ratio can additionally be partially altered by elemental sulfur deposition (Figure 7).

The magmatic CO_2/S_T signature of the Minas de Azufre volcanic gas that we bring to light is relatively unique. Indeed, the majority of caldera-hosted fumarolic systems (e.g., Campi Flegrei; Chiodini et al., 2016; Yellowstone; Bergfeld et al., 2011; Hurwitz & Lowenstern, 2014) tend to exhibit S-depleted hydrothermal gas signatures, owing to extensive loss of magmatic S through scrubbing and deposition in the subsurface. We note that our gas measurements in October 2017 were performed only ∼9 months before the onset of the June-August 2018 eruption at Sierra Negra, when both seismicity and ground deformation were entering an escalating phase (Bell et al., 2021).Therefore, it is possible that the heightened seismicity/ground uplift contributed to more efficient TDF-mediated transport of magmatic volatiles from the sill at that time. Instead, the comparatively higher H_2O content of Minas de Azufre fumaroles in 1995 (Goff et al., 2000) and 2006 (Padrón et al., 2012; see Figures 4 and 6) suggests enhanced meteoric dilution of the upraising magmatic gas, and thus enhanced possibility of its hydrothermal alteration, during the post-eruptive phases or quiescent periods. In these phase more remote from eruptions, the reduced magmatic gas supply is supported by ground subsidence (Geist et al., 2006). However, the relatively steady "magmatic" CO_2/S_T ratio observed by Taran et al. (2010) in 2004 (Figure 6), one year before the October 2005 eruption (Geist et al., 2008), implies that the gas conditions encountered in October 2017 are not exceptional. We conclude that the unusually shallow depth (∼2 km) of magma storage beneath the Sierra Negra caldera provides favorable conditions for a rapid transit of magmatic gases to the surface, thereby preventing their hydrothermal alteration. We therefore suggest that implementing a continuous gas monitoring at Minas de Azufre could be highly beneficial to improve volcanic hazard assessment and eruption forecasting at Sierra Negra volcano.

Data Availability Statement

All processed data generated or analysed during this study are included in Tables 1 and 2. The raw Multi-GAS data set (used to generate Figure 2) and the processed UV Camera data set (used to generate Figure 3) are also publicly available in the EarthChem data library (ECL) repository (https://www.earthchem.org/ecl/) (Aiuppa et al., 2022). The CO_2-H_2O-SO_2-H_2S-melt saturation and degassing code (Moretti et al., 2003; Moretti & Papale, 2004) is publicly available for download at https://github.com/charlesll//chosetto (doi: https://doi.org/10.5281/zenodo.5554941). The CHOSETTO.exe program (for Windows®) is available together with instructions to run it and relevant information on licensing and credits to be given.

Acknowledgments
The authors wish to thank the PNG (Galápagos National Park) for help and support provided during the field activity. Constructive reviews by Dennis Geist, Yuri Taran and one anonymous reviewer helped improving the manuscript. This study was conducted within the frame of the "Convenio de cooperación PNG-IG-EPN." Alessandro Aiuppa received funding from the Deep Carbon Observatory (subcontract no. 10759–1238) and from the Italian Ministero Istruzione Università e Ricerca (Miur, Grant N. 2017LMNLAW).

References

Aiuppa, A. (2015). Volcanic gas monitoring. In A. Schmidt, K. E. Fristad, & L. T. Elkins-Tanton (Eds.), *Volcanism and global environmental change* (pp. 81–96). Cambridge University Press.

Aiuppa, A., Allard, P., Bernard, B., Lo Forte, F. M., Moretti, R., & Hidalgo, S. (2022). Volcanic gas plume compositions and SO_2 flux from Minas de Azufre, Sierra Negra Volcano (Ecuador), version 1.0. *Interdisciplinary Earth data alliance (IEDA)*. https://doi.org/10.26022/IEDA/112195

Aiuppa, A., Bani, P., Moussallam, Y., Di Napoli, R., Allard, P., Gunawan, H., et al. (2015). First determination of magma-derived gas emissions from Bromo volcano, eastern Java (Indonesia). *Journal of Volcanology and Geothermal Research*, *304*, 206–213. https://doi.org/10.1016/j.jvolgeores.2015.09.008

Aiuppa, A., Bertagnini, A., Métrich, N., Moretti, R., Di Muro, A., Liuzzo, M., & Tamburello, G. (2010). A degassing model for Stromboli volcano. *Earth and Planetary Science Letters*, *295*, 195–204. https://doi.org/10.1016/j.epsl.2010.03.040

Aiuppa, A., Bitetto, M., Francofonte, V., Velasquez, G., Bucarey Parra, C., Giudice, G., et al. (2017). A CO_2-gas precursor to the arch 2015 Villarrica volcano eruption. *Geochemistry, Geophysics, Geosystems*, *18*, 2120–2132. https://doi.org/10.1002/2017GC006892

Aiuppa, A., Casetta, F., Coltorti, M., Stagno, V., & Tambuerllo, G. (2021). Carbon concentration increases with depth of melting in Earth's upper mantle. *Nature Geoscience*, *14*, 697–703. https://doi.org/10.1038/s41561-021-00797-y

Aiuppa, A., Federico, C., Giudice, G., & Gurrieri, S. (2005). Chemical mapping of a fumarolic field: La Fossa Crater, Vulcano Island (Aeolian Islands, Italy). *Geophysical Research Letters*, *32*(13), 1–4. https://doi.org/10.1029/2005gl023207

Aiuppa, A., Moretti, R., Federico, C., Giudice, G., Gurrieri, S., Liuzzo, M., et al. (2007). Forecasting Etna eruptions by real-time observation of volcanic gas composition. *Geology*, *35*(12), 1115–1118. https://doi.org/10.1130/g24149a.1

Amelung, F., Jónsson, S., Zebker, H., & Segall, P. (2000). Widespread uplift and "trapdoor" faulting on Galapagos volcanoes observed with radar interferometry. *Nature*, *407*, 993–996. https://doi.org/10.1038/35039604

Bell, A. F., La Femina, P. C., Ruiz, M., Amelung, F., Bagnardi, M., Bean, C. J., et al. (2021). Caldera resurgence during the 2018 eruption of Sierra Negra volcano, Galápagos Islands. *Nature Communications*, *12*, 1397. https://doi.org/10.1038/s41467-021-21596-4

Bergfeld, D., Lowenstern, J. B., Hunt, A. G., Shanks, W. C. P., III, & Evans, W. C. (2011). Gas and isotope chemistry of thermal features in Yellowstone National Park, Wyoming. *U.S. Geological Survey Scientific Investigations Report 2011–5012*, 28. https://doi.org/10.3133/sir20115012

Caricchi, L., Sheldrake, T. E., & Blundy, J. (2018). Modulation of magmatic processes by CO_2 flushing. *Earth and Planetary Science Letters*, *491*, 160–171. https://doi.org/10.1016/j.epsl.2018.03.042

Chadwick, W. W., Geist, D. J., Jonsson, S., Poland, M. P., Johnson, D. J., & Meertens, C. M. (2006). A volcano bursting at the seams: Inflation, faulting, and eruption at Sierra Negra volcano, Galápagos. *Geology*, *34*(12). https://doi.org/10.1130/g22826a.1

Chiodini, G., & Marini, L. (1998). Hydrothermal gas equilibria: The H_2O–H_2–CO_2–CO–CH_4 system. *Geochimica et Cosmochimica Acta*, *62*, 2673–2687. https://doi.org/10.1016/S0016-7037(98)00181-1

Chiodini, G., Paonita, A., Aiuppa, A., Costa, A., Caliro, S., De Martino, P., et al. (2016). Magmas near the critical degassing pressure drive volcanic unrest towards a critical state. *Nature Communications*, *7*, 13712. https://doi.org/10.1038/ncomms13712

Colony, W. E., & Nordlie, B. E. (1973). Liquid sulfur at Volcano Azufre, Galapagos Islands. *Economic Geology Series*, *68*, 371–380. https://doi.org/10.2113/gsecongeo.68.3.371

Dasgupta, R., & Hirschmann, M. M. (2010). The deep carbon cycle and melting in Earth's interior. *Earth and Planetary Science Letters*, *298*, 1–13. https://doi.org/10.1016/j.epsl.2010.06.039

de Moor, J. M., Aiuppa, A., Avard, G., Wehrmann, H., Dunbar, N., Muller, C., et al. (2016). Turmoil at Turrialba volcano (Costa Rica): Degassing and eruptive behavior inferred from high frequency gas monitoring. *Journal of Geophysical Research*, *121*(8), 5761–5775. https://doi.org/10.1002/2016jb013150

de Moor, J. M., Fischer, T. P., Sharp, Z. D., King, P. L., Wilke, M., Botcharnikov, R. E., et al. (2013). Sulfur degassing at Erta Ale (Ethiopia) and Masaya (Nicaragua) volcanoes: Implications for the degassing processes and oxygen fugacities of basaltic systems. *Geochemistry, Geophysics, Geosystems*, *14*, 4076–4108. https://doi.org/10.1002/ggge.20255

Delle Donne, D., Aiuppa, A., Bitetto, M., D'Aleo, R., Coltelli, M., Coppola, D., et al. (2019). Changes in SO_2 flux regime at Mt. Etna captured by automatically processed ultraviolet camera data. *Remote Sensing*, *11*, 1201. https://doi.org/10.3390/rs11101201

Edmonds, M., Aiuppa, A., Humphreys, M., Moretti, R., Giudice, G., Martin, R., et al. (2010). Excess volatiles supplied by mingling of mafic magma at an andesitic arc volcano. *Geochemistry, Geophysics, Geosystems*, *11*(4), Q04005. https://doi.org/10.1029/2009GC002781

Fischer, T. P. (2008). Fluxes of volatiles (H_2O, CO_2, N_2, Cl, F) from arc volcanoes. *Geochemistry Journal*, *42*(1), 21–38. https://doi.org/10.2343/geochemj.42.21

Fischer, T. P., Arellano, S., Carn, S., Aiuppa, A., Galle, B., Allard, P., et al. (2019). The emissions of CO_2 and other volatiles from the world's subaerial volcanoes. *Scientific Reports*, *9*(1), 18716. https://doi.org/10.1038/s41598-019-54682-1

Fischer, T. P., & Chiodini, G. (2015). Volcanic, magmatic and hydrothermal gas discharges. In H. Sigurdsson, B. Houghton, S. McNutt, H. Rymer, & J. Stix (Eds.), *Encyclopaedia of volcanoes* (2nd ed., pp. 779–797). Academic Press. https://doi.org/10.1016/b978-0-12-385938-9.00045-6

Geist, D., Chadwick, W., & Johnson, D. (2006). Results from new GPS and gravity monitoring networks at Fernandina and Sierra Negra Volcanoes, Galápagos, 2000-2002. *Journal of Volcanology and Geothermal Research*, *150*(1–3), 79–97. https://doi.org/10.1016/j.jvolgeores.2005.07.003

Geist, D. J., Harpp, K. S., Naumann, T. R., Poland, M., Chadwick, W. W., Hall, M., & Rader, E. (2008). The 2005 eruption of Sierra Negra volcano, Galápagos, Ecuador. *Bulletin of Volcanology*, *70*, 655–673. https://doi.org/10.1007/s00445-007-0160-3

Geist, D. J., White, W. M., & McBirney, A. R. (1988). Plume-asthenosphere mixing beneath the Galapagos archipelago. *Nature*, *333*, 657–660. https://doi.org/10.1038/333657a0

Gerlach, T. M. (1982). Interpretation of volcanic gas data from tholeiitic and alkaline mafic lavas. *Bulletin of Volcanology*, *45*, 235–244. https://doi.org/10.1007/bf02597736

Gerlach, T. M., & Graeber, E. J. (1985). Volatile budget of Kilauea Volcano. *Nature*, *313*, 273–277. https://doi.org/10.1038/313273a0

Gibson, S. A., Geist, D. G., Day, J. A., & Dale, C. W. (2012). Short wavelength heterogeneity in the Galápagos plume: Evidence from compositionally diverse basalts on Isla Santiago. *Geochemistry, Geophysics, Geosystems*, *13*, Q09007. https://doi.org/10.1029/2012gc004244

Giggenbach, W. F. (1987). Redox processes governing the chemistry of fumarolic gas discharges from White Island, New Zealand. *Applied Geochemistry*, *2*(2), 143–161. https://doi.org/10.1016/0883-2927(87)90030-8

Giggenbach, W. F. (1996). Chemical composition of volcanic gases. In R. Scarpa, & R. Tilling (Eds.), *Monitoring and mitigation of volcano hazard* (pp. 221–256). Springer Verlag. https://doi.org/10.1007/978-3-642-80087-0_7

Gleeson, M. L. M., Gibson, S. A., Stock, M. J., & EIMF. (2022). Constraints on the behaviour and content of volatiles in Galápagos magmas from melt inclusions and nominally anhydrous minerals. *Geochimica et Cosmochimica Acta*, *319*, 168–190. https://doi.org/10.1016/j.gca.2021.11.005

Goff, F., McMurtry, G. M., Counce, D., Simac, J. A., Roldan-Manzo, A. R., & Hilton, D. R. (2000). Contrasting hydrothermal activity at Sierra Negra and Alcedo volcanoes, Galapagos Archipelago, Ecuador. *Bulletin of Volcanology*, *62*, 34–52. https://doi.org/10.1007/s004450050289

Harpp, K. S., & Geist, D. J. (2018). The evolution of Galápagos Volcanoes: An alternative perspective. *Frontiers of Earth Science*, *6*(50). https://doi.org/10.3389/feart.2018.00050

Harpp, K. S., Mittelstaedt, E., d'Ozouville, N., & Graham, D. W. (2014). *The Galápagos: A natural laboratory for the Earth sciences*. In *Geophysical Monograph 204*. American Geophysical Union.

Harpp, K. S., & White, W. M. (2001). Tracing a mantle plume: Isotopic and trace element variations of Galápagos seamounts. *Geochemistry, Geophysics, Geosystems*, *2*(6), 1042. https://doi.org/10.1029/2000GC000137

Hauri, E. H., Cottrell, E., Kelley, K. A., Tucker, J. M., Shimizu, K., Le Voyer, M., et al. (2019). Carbon in the convecting mantle. In B. N. Orcutt, I. Daniel, & R. Dasgupta (Eds.), *Deep carbon, past to present* (pp. 237–275). Cambridge Univ. Press. https://doi.org/10.1017/9781108677950.009

Hernández, P. A., Melián, G. V., Dionis, S., Barrancos, J., Padilla, G., Padrón, E., et al. (2015). Chemical composition of volcanic gases emitted during the 2014-15 Fogo eruption, Cape Verde. *Geophysical Research Abstracts*, *17*, EGU2015–9577. EGU General Assembly 2015.

Hidalgo, S., Bernard, B., Hasselle, N., Narvaez, D., & Vásconez, F. (2014). Medición de gases y temperatura en la zona fumarólica de Minas de Azufre - volcán Sierra Negra (Isla Isabela - Galápagos). IGEPN Internal report.

Hofmann, A. W. (2003). Sampling mantle heterogeneity through oceanic basalts: Isotopes and trace elements. In H. D. Holland & K. K. Turekian (Eds.), *Treatise on Geochemistry*. *The mantle and core* (Vol. 2, pp. 61–101). Elsevier.

Hooft, E. E., Toomey, D. R., & Solomon, S. C. (2003). Anomalously thin transition zone beneath the Galápagos hotspot. *Earth and Planetary Science Letters*, *216*, 55–64. https://doi.org/10.1016/s0012-821x(03)00517-x

Hurwitz, S., & Lowenstern, J. B. (2014). Dynamics of the Yellowstone hydrothermal system. *Review of Geophysics*, *51*, 375–411. https://doi.org/10.1002/2014RG000452

Jónsson, S., Zebker, H., & Amelung, F. (2005). On trapdoor faulting at Sierra Negra volcano, Galápagos. *Journal of Volcanology and Geothermal Research*, *144*, 59–71. https://doi.org/10.1016/j.jvolgeores.2004.11.029

Koleszar, A. M., Saal, A. E., Hauri, E. H., Nagle, A. N., Liang, Y., & Kurz, M. D. (2009). The volatile contents of the Galápagos plume; evidence for H_2O and F open system behavior in melt inclusions. *Earth and Planetary Science Letters*, *287*(3–4), 442–452. https://doi.org/10.1016/j.epsl.2009.08.029

Kurz, M. D., Curtice, J., Fornari, D., Geist, D. J., & Moreira, M. (2009). Primitive neon from the center of the Galápagos hotspot. *Earth and Planetary Science Letters*, *286*(1–2), 23–34. https://doi.org/10.1016/j.epsl.2009.06.008

Kurz, M. D., & Geist, D. J. (1999). Dynamics of the Galápagos hotspot from helium isotope geochemistry. *Geochimica et Cosmochimica Acta*, *63*(23–24), 4139–4156. https://doi.org/10.1016/S0016-7037(99)00314-2

Kurz, M. D., Rowland, S., Curtice, J., Saal, A., & Naumann, T. (2014). Eruption rates for Fernandina volcano: A new chronology at the Galápagos hotspot center. In K. S. Harpp, E. Mittelstaedt, N. d'Ozouville, & D. W. Graham (Eds.), *The Galápagos: A natural Laboratory for the Earth sciences, geophysical monograph 204* (pp. 41–54). American Geophysical Union. https://doi.org/10.1002/9781118852538.ch4

Lages, J., Moussallam, Y., Bani, P., Peters, N., Aiuppa, A., Bitetto, M., & Giudice, G. (2020). First in-Situ measurements of plume chemistry at mount Garet Volcano, Island of Gaua (Vanuatu). *Applied Sciences*, *10*, 7293. https://doi.org/10.3390/app10207293

Marini, L., Moretti, R., & Accornero, M. (2011). Sulfur isotopes in magmatic-hydrothermal systems, melts, and Magma. *Reviews in Mineralogy and Geochemistry*, *58*, 423–492. https://doi.org/10.2138/rmg.2011.73.14

Moretti, R., Arienzo, I., Civetta, L., Orsi, G., & D'Antonio, M. (2013). The deep plumbing system of the Ischia Island: A physico-chemical window on the fluid-saturated and CO_2-sustained Neapolitan volcanism (southern Italy). *Journal of Petrology*, *54*, 951–984. https://doi.org/10.1093/petrology/egt002

Moretti, R., Arienzo, I., Civetta, L., Orsi, G., & Papale, P. (2013). Multiple magma degassing sources at an explosive volcano. *Earth and Planetary Science Letters*, *367*, 95–104. https://doi.org/10.1016/j.epsl.2013.02.013

Moretti, R., Métrich, N., Arienzo, I., Di Renzo, V., Aiuppa, A., & Allard, P. (2018). Degassing vs. eruptive styles at Mt. Etna volcano (Sicily, Italy). Part I: Volatile stocking, gas fluxing, and the shift from low-energy to highly explosive basaltic eruptions. *Chemical Geology*, *482*, 1–17. https://doi.org/10.1016/j.chemgeo.2017.09.017

Moretti, R., & Papale, P. (2004). On the oxidation state and volatile behavior in multicomponent gas melt equilibria. *Chemical Geology*, *213*, 265–280. https://doi.org/10.1016/j.chemgeo.2004.08.048

Moretti, R., Papale, P., & Ottonello, G. (2003). A model for the saturation of C-H-O-S fluids in silicate melts. In C. Oppenheimer, D. M. Pyle, & J. Barclay (Eds.), (Vol. 213, pp. 81–101). Geological Society of London Special Publication. *Volcanic Degassing*. https://doi.org/10.1144/gsl.sp.2003.213.01.06

Moussallam, Y., Longpré, M. A., McCammond, C., Gomez-Ulla, A., Rose-Koga, E. F., Scaillet, B., et al. (2019). Mantle plumes are oxidised. *Earth and Planetary Science Letters*, *527*, 115798. https://doi.org/10.1016/j.epsl.2019.115798

Oppenheimer, C., Fischer, T. P., & Scaillet, B. (2014). Volcanic degassing: Process and impact. In H. D. Holland & K. K. Turekian (Eds.), *Treatise on Geochemistry. The mantle and core* (Vol. 2, pp. 111–179). Elsevier. https://doi.org/10.1016/b978-0-08-095975-7.00304-1

Oppenheimer, C., Moretti, R., Kyle, P., Eschenbacher, A., Lowenstern, J., Hervig, G., & Dunbar, N. (2011). Mantle to surface gas trigger of the alkalic intraplate Erebus volcano, Antarctica. *Earth and Planetary Science Letters*, *306*, 261–271. https://doi.org/10.1016/j.epsl.2011.04.005

Padrón, E., Hernández, P. A., Pérez, N. M., Toulkeridis, T., Melián, G., Barrancos, J., et al. (2012). Fumarole/plume and diffuse CO_2 emission from Sierra Negra caldera, Galapagos archipelago. *Bulletin of Volcanology*, *70*, 1509–1519. https://doi.org/10.1007/s00445-012-0610-4

Papale, P., Moretti, R., & Barbato, D. (2006). The compositional dependence of the saturation surface of H_2O+CO_2 fluids in silicate melts. *Chemical Geology*, *229*, 78–95. https://doi.org/10.1016/j.chemgeo.2006.01.013

Peterson, M. E., Kelley, K. A., Cottrell, E., Saal, A. E., & Kurz, M. D. (2015). *The oxidation state of Fe in glasses from the Galápagos archipelago: Variable oxygen fugacity as a function of mantle source*. American Geophysical Union (AGU) Fall Meeting. abstract # V23E-03.

Peterson, M. E., Saal, A. E., Kurz, M. D., HauriE Blusztajn, J. S., Harpp, K. S., Werner, R., et al. (2017). Submarine basaltic glasses from the Galápagos Archipelago: Determining the volatile budget of the mantle plume. *Journal of Petrology*, *58*(7), 1419–1450. https://doi.org/10.1093/petrology/egx059

Pfeffer, M., Bergsson, B., Barsotti, S., Stefánsdóttir, G., Galle, B., Arellano, S., et al. (2018). Ground-based measurements of the 2014–2015 Holuhraun Volcanic cloud (Iceland). *Geosciences*, *8*, 29. https://doi.org/10.3390/geosciences8010029

Pino, A. N., Moretti, R., Allard, P., & Bischi, E. (2011). Seismic precursors of a basaltic paroxysmal explosion track deep gas accumulation and slug upraise. *Journal of Geophysical Research*, *116*(B2). https://doi.org/10.1029/2009JB000826

Reynolds, R. W., & Geist, D. J. (1995). Petrology of lavas from Sierra Negra volcano, Isabela Island, Galápagos archipelago. *Journal of Geophysical Research*, *100*(B12), 24553–24537. https://doi.org/10.1029/95JB02809

Reynolds, R. W., Geist, D. J., & Kurz, M. D. (1995). Physical volcanology and structural development of Sierra Negra volcano, Isabela Island, Galapagos Archipelago. *Bulletin of the Geological Society of America*, *107*, 1398–1410. https://doi.org/10.1130/0016-7606(1995)107<1398:pvasdo>2.3.co;2

Sawyer, G. M., Oppenheimer, C., Tsanev, V. I., & Yirgu, G. (2008). Magmatic degassing at Erta'Ale volcano, Ethiopia. *Journal of Volcanology and Geothermal Research*, *178*, 837–846. https://doi.org/10.1016/j.jvolgeores.2008.09.017

Shinohara, H. (2005). A new technique to estimate volcanic gas composition: Plume measurements with a portable multi-sensor system. *Journal of Volcanology and Geothermal Research*, *143*, 319–333. https://doi.org/10.1016/j.jvolgeores.2004.12.004

Sigvaldsson, G. E., & Elisson, G. (1968). Collection and analysis of volcanic gases at Surtsey, Iceland. *Geochimica et Cosmochimica Acta*, *32*, 797–805.

Spilliaert, N., Allard, P., Métrich, N., & Sobolev, A. (2006). Melt inclusion record of the conditions of ascent, degassing and eruption of primitive alkali basalt during the powerful 2002 flank eruption of Mount Etna. *Journal of Geophysical Research: Solid Earth*, *111*, B04203. https://doi.org/10.1029/2005JB003934

Stix, J., & de Moor, J. M. (2018). Understanding and forecasting phreatic eruptions driven by magmatic degassing. *Earth Planets and Space*, *70*, 83. https://doi.org/10.1186/s40623-018-0855-z

Sutton, A. J., & Elias, T. (2014). One hundred volatile years of Volcanic gas studies at the Hawaiian Volcano observatory. In M. P. Poland, T. J. Takahashi, & C. M. Landowski (Eds.), *Characteristics of Hawaiian volcanoes. US geological survey professional paper 1801* (pp. 295–320). USGS, 2014). https://doi.org/10.3133/pp18017

Symonds, R. B., Rose, W. I., Bluth, G. J. S., & Gerlach, T. M. (1994). Volcanic-gas studies: Methods, results and applications. *Reviews in Mineralogy*, *30*, 1–66. https://doi.org/10.1515/9781501509674-007

Tamburello, G. (2015). Ratiocalc: Software for processing data from multicomponent volcanic gas analyzers. *Computers & Geosciences*, *82*, 63–67. https://doi.org/10.1016/j.cageo.2015.05.004

Tamburello, G., Kantzas, E. P., McGonigle, A. J. S., & Aiuppa, A. (2011). Vulcamera: A program for measuring volcanic SO_2 using UV cameras. *Annales de Geophysique*, *54*(2), 219–221. https://doi.org/10.4401/ag-5181

Taran, Y., Christenson, B., Sumino, H., & Kennedy, B. (2010). *Gas geochemistry of Sierra Negra volcano, Galapagos hot spot*. American Geophysical Union (AGU) Fall Meeting. abstract #V41A-2266.

Taran, Y., & Zelenski, M. (2015). Systematics of water isotopic composition and chlorine content in arc-volcanic gases. In G. F. Zellmer, M. Edmonds, & S. M. Straub (Eds.), *The Role of Volatiles in the Genesis, Evolution and Eruption of Arc Magmas*. Geological Society, London, Special Publications (Vol. 410, pp. 237–262). https://doi.org/10.1144/sp410.5

Vasconez, F. J., Ramón, P., Hernandez, S., Hidalgo, S., Bernard, B., Ruiz, M., et al. (2018). The different characteristics of the recent eruptions of Fernandina and Sierra Negra volcanoes (Galápagos, Ecuador). *Volcanica*, *1*(2), 127–133. https://doi.org/10.30909/vol.01.02.127133

Vigouroux, N., Williams-Jones, G., Chadwick, W., Geist, D., Ruiz, A., & Johnson, D. (2008). 4D gravity changes associated with the 2005 eruption of Sierra Negra volcano, Galápagos. *Geophysics*, *73*(6), WA29–WA35. https://doi.org/10.1190/1.2987399

Villagómez, D. R., Toomey, D. R., Hooft, E. E., & Solomon, S. C. (2007). Upper mantle structure beneath the Galápagos Archipelago from surface wave tomography. *Journal of Geophysical Research*, *112*, B07303. https://doi.org/10.1029/2006JB004672

White, W. M., McBirney, A. R., & Duncan, R. A. (1993). Petrology and geochemistry of the Galapagos Islands: Portrait of a pathological mantle plume. *Journal of Geophysical Research*, *98*, 19533–19563. https://doi.org/10.1029/93jb02018

Zelenski, M., Fischer, T. P., de Moor, J. M., Marty, B., Zimmermann, L., Ayalew, D., et al. (2013). Trace elements in the gas emissions from the Erta Ale volcano, Afar, Ethiopia. *Chemical Geology*, *357*, 95–116. https://doi.org/10.1016/j.chemgeo.2013.08.022

Zindler, A., & Hart, S. (1986). Chemical geodynamics. *Annual Review of Earth and Planetary Sciences*, *14*, 493–571. https://doi.org/10.1146/annurev.ea.14.050186.002425